Supporting Information

Tailored Spacer Molecule in 2D/3D Heterojunction for Ultralow-Voltage-Loss and Stable Perovskite Solar Cells

Weili Fan[1], Ying Shen[2], Kaimo Deng[2], Qinghua Chen[2], and Yang Bai[1*]*

[1] Beijing Advanced Innovation Center for Materials Genome Engineering, Institute for Advanced Materials and Technology, University of Science and Technology Beijing, Beijing 100083, P. R. China

[2] School of Physical Science and Technology, Jiangsu Key Laboratory of Thin Films, Soochow University, Suzhou 215006, P. R. China

E-mail: baiy@mater.ustb.edu.cn; dkm@suda.edu.cn

Experimental section

Materials: dimethylformamide (DMF), dimethyl sulfoxide (DMSO), Chlorobenzene (CB) and isopropyl alcohol (IPA) were purchased from Sigma-Aldrich. SnO_2 colloid solution (tin (IV) oxide, 15 % in H_2O colloidal dispersion) was purchased from Alfa Aesar. Formamidine iodide (FAI) was purchased from GreatCell Solar Lead(II) iodide (PbI_2), methylammonium bromide (MABr), $PbBr_2$, CsI, RbI, 2,2′,7,7′-tetrakis (N,N-di-p-methoxyphenylamine)-9,9'-spirobifl-uorene (spiro-OMeTAD) and bis(trifluoro-methane) sulfonimide lithium salt (Li-TFSI) were purchased from Xi'an Polymer Light Technology Corp. 4-tert-butylpyridine (TBP) was purchased from Macklin.

Synthesis of 4-hydroxy-phenylethylamine iodide (OH-PEAI): 4-hydroxy-phenylethylamine (Aladdin, 1 g) was dissolved in ethanol (Aladdin, 5 mL) and hydroiodide acid (Sigma, 57 wt%, 1.2 mL) was added dropwise under magnetic stirring for 30 min. After conducting the recrystallization process using diethyl ether, the precipitate was collected by filtration and washed with diethyl ether and then dried under vacuum to afford OH-PEAI as a crystalline light yellow solid.

Device Fabrication: The diluted SnO_2 precursor solution (3 wt%) was spin coated onto cleaned ITO glass at 5000 rpm for 20 s, and then annealed at 150 ℃ for 30 min. The ITO/SnO_2 substrate were treated with UV light before transferred into glove box for perovskite deposition. The $Rb_{0.05}Cs_{0.05}[(FA_{0.83}MA_{0.17})]_{0.9}Pb(I_{0.83}Br_{0.17})_3$ perovskite layer with a bandgap of 1.61 eV was fabricated by one-step method. PbI_2 (1.1 M), $PbBr_2$ (0.22 M), FAI (1 M) and MABr (0.2 M) were dissolved in a mixed solution of DMF/DMSO (4:1, v:v), then 50 μL CsI stock solution (1.5 M in DMSO) and 50 μL RbI (1.5 M in DMSO) solution were added. The perovskite precursor solution was spin-coated at 1000 rpm for 10 s (200 rpm ramp), and 6000 rpm for 30 s (2000 rpm ramp). After 5 s into the 6000 rpm setting, 150 μL CB was dropped onto the

substrate. Afterwards, the ITO/SnO_2/perovskite substrates were annealed at 105 °C for 30 min. The $Cs_{0.05}FA_{0.85}MA_{0.10}Pb(I_{0.97}Br_{0.03})_3$ perovskite layer with a bandgap of 1.56 eV was fabrication by one-step method. PbI_2 (1.6 M), FAI (1.3 M), and MABr (0.14 M) were dissolved in a mixed solution of DMF/DMSO (4:1, v:v), then 50 μL CsI stock solution (1.5 M in DMSO) solution was added. The perovskite precursor solution was spin-coated at 1000 rpm for 10 s (200 rpm ramp), and 5000 rpm for 40 s (2000 rpm ramp). After 5 s into the 5000 rpm setting, 150 μL CB was dropped onto the substrate. Afterwards, the ITO/SnO_2/perovskite substrates were annealed at 120 °C for 20 min. To deposit the OH-PEAI passivation layer, OH-PEAI was dissolved in IPA with different concentrations (2, 4 and 6 mg mL^{-1}) and then spin-coated on the 3D perovskite surface at 5000 rpm for 30 s without additional annealing treatment. After the substrates were cooled to room temperature, 20 μL Spiro-OMeTAD solution was spin-coated at 2000 rpm for 30 s, and it contains 72.3 mg Spiro-OMeTAD, 29 μL of 4-tert-butylpyridine (TBP), 35 μL of bis(trifluoromethane) sulfonimide lithium salt (Li-TFSI) solution (260 mg mL^{-1} in acetonitrile) in 1 mL chlorobenzene. Finally, the Ag electrode (90 nm) was deposited by thermal evaporated.

Device Characterization: The structure of perovskite was characterized by an X-ray diffractometer (XRD) (D/MAX-III-B-40KV, Cu Kα radiation, λ = 0.15418 nm) and X-ray photoemission spectroscopy (XPS, ESCALAB 250Xi, Thermo Fisher Scientific), respectively. Scanning electron microscopy (SEM, SU8010, Hitachi) and atomic force microscopy (AFM, Multimode 8, BRUKER) were performed to characterize the morphology of the perovskite films. Kelvin probe force microscopy (KPFM) is used for surface potential measurements with amplitude modulated mode. The absorption spectra were characterized by the UV-visible spectrophotometer (UV-3600, Shimadzu Corp.). The photoluminescence (PL) spectra and time-resolved photoluminescence (TRPL) spectra were recorded by a spectrofluorometer

(Edinburgh FLS1000). Fourier transform infrared (FT-IR) spectroscopy was measured by a Fourier infrared spectrometer (NICOLET 6700, BRUKER). The contact angle of water droplets on the surfaces of the perovskite film was characterized by a digital camera (DAHENG IMAGING, DH-HV1351UM). The current density-voltage (*J-V*) curves were measured by using a Keithley 2400 Source Meter with a Newport solar simulator (AM 1.5G irradiation, 100 mW/cm^2). The active area of the PSCs was 0.11 cm^{-2} defined by a metal shadow mask. The electrochemical impedance spectroscopy (EIS) was carried by an electrochemical workstation (Autolab PGSTAT302N, Metrohm AG) under AM 1.5G illumination with an alternative signal amplitude of 5 mV and a frequency range of 800-0.01 kHz. Confocal laser scanning microscopy (CLSM) images were measured on Zeiss LSM510 confocal laser scanning microscopy under ambient air conditions with the excitation at 458nm and the emission wavelength at 708-719 nm of 3D perovskite and 505-676 nm of 2D perovskite.

Theoretical calculation: The density functional theory (DFT) calculation was performed by the Cambridge serial total energy package code and a plane wave basis set was used. The exchange and correlation interactions were modeled using the generalized gradient approximation and the Perdew-Burke-Ernzerhof function. Grimme's semi-empirical DFT-D was chosen in the computations to guarantee a better description of the electron interaction in a long range. The Vanderbilt ultrasoft pseudopotential was used with a cutoff energy of 500 eV. Geometric convergence tolerances were set for a maximum force of 0.03 eV/A˚, a maximum energy change of 10^{-5} eV/atom, a maximum displacement of 0.001 A˚, and a maximum stress of 0.5 GPa. Density mixing electronic minimisation was implemented and the self-consistent field tolerance was set to ''fine'' with a high accuracy of 10^{-6} eV/atom for energy convergence.

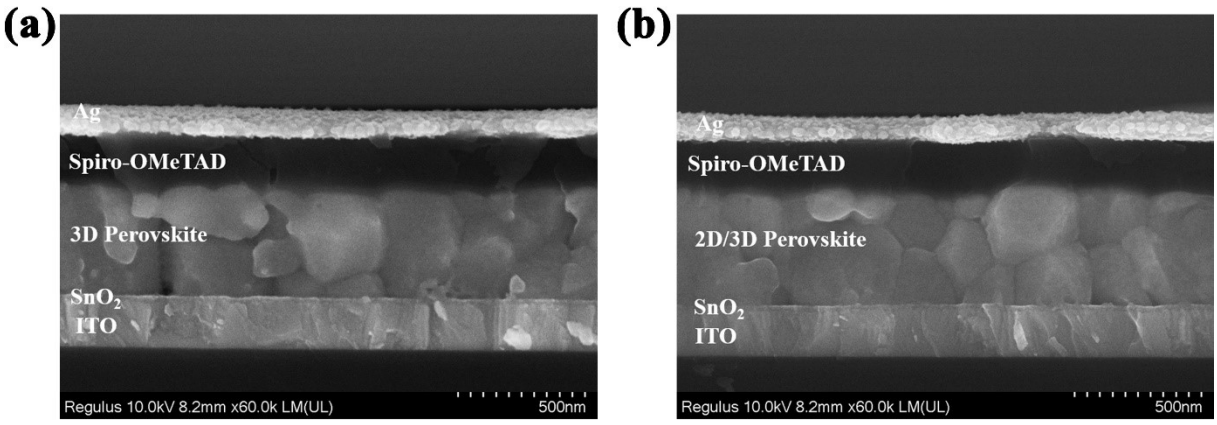

Fig. S1 Cross-section scanning electron microscopy (SEM) images for 3D (a) and 2D/3D (b) PSCs.

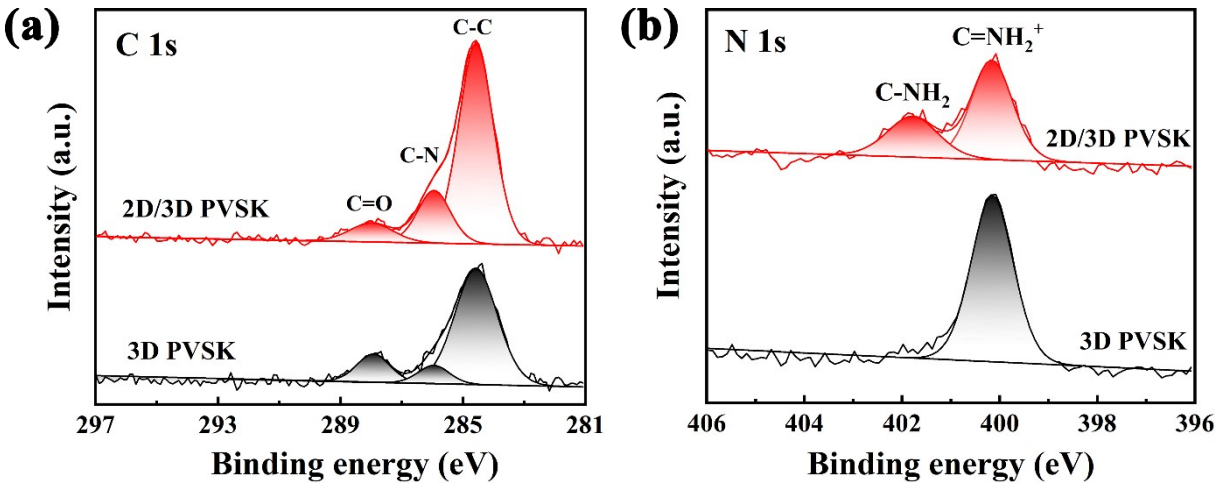

Fig. S2 XPS of C 1s and N 1s spectra for 3D and 2D/3D perovskite films.

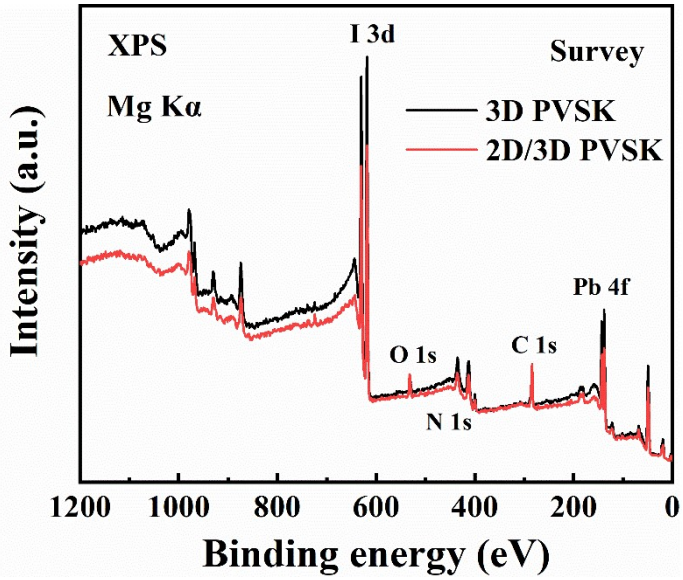

Fig. S3 XPS survey scans for 3D and 2D/3D perovskite films.

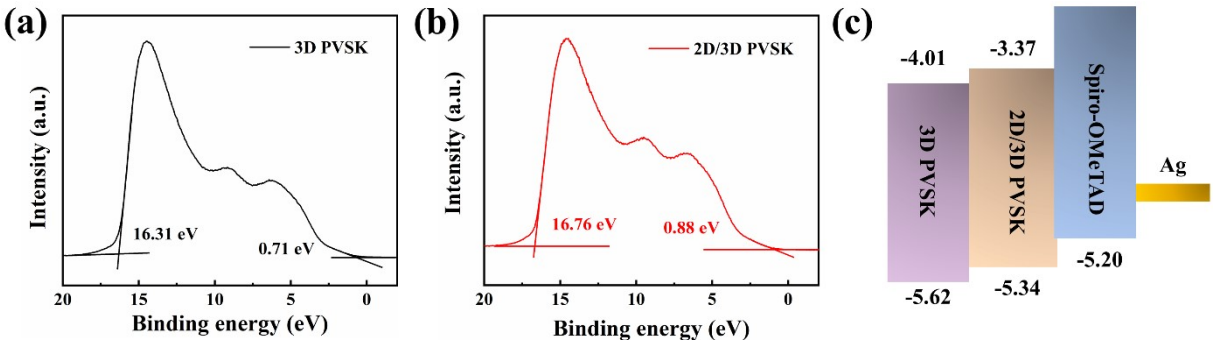

Fig. S4 UPS spectra 3D perovskite (a) and 2D/3D perovskite (b) and the energy diagram of the 2D/3D and 3D perovskite films.

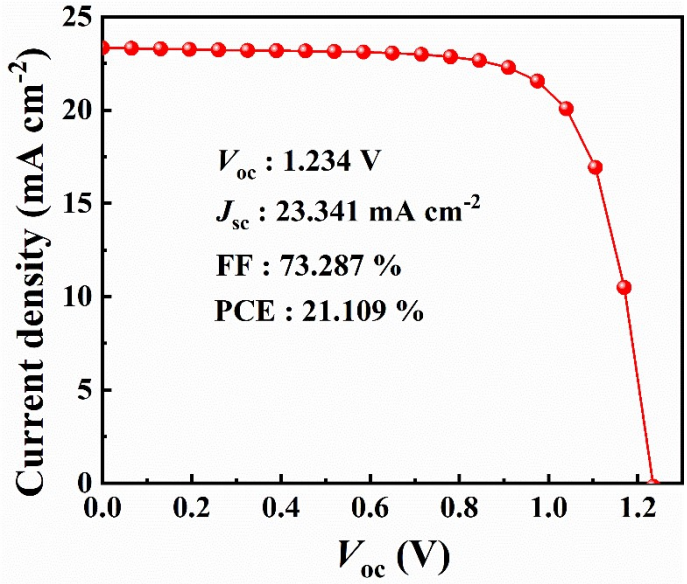

Fig. S5 *J-V* curve of 2D/3D PSCs with a V_{oc} of 1.234 V.

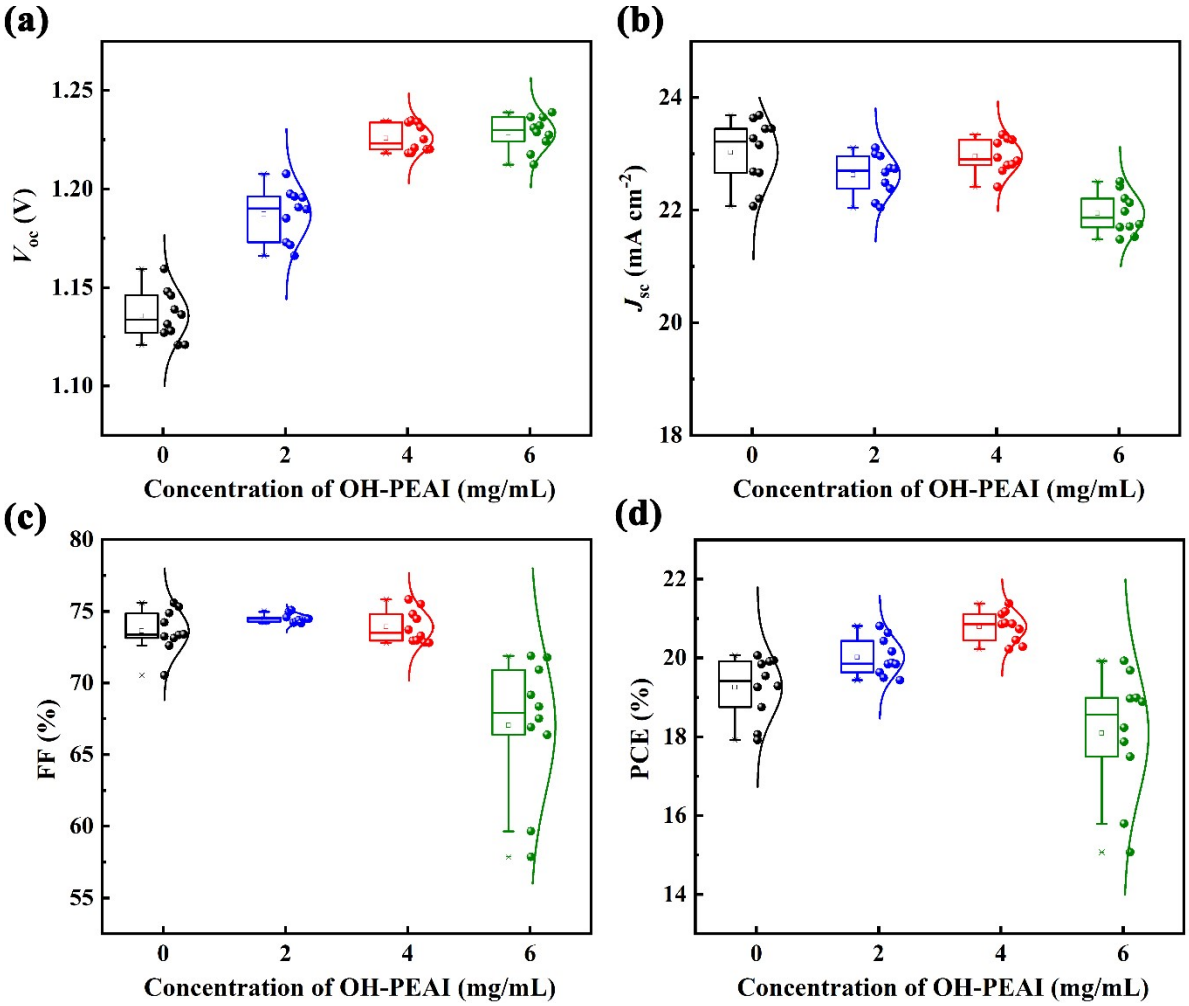

Fig. S6 Statistic distribution of photovoltaic parameters for the 2D/3D and 3D PSCs with different concentrations of OH-PEAI (0, 2, 4, and 6 mg/mL): (a) V_{oc}, (b) J_{sc}, (c) FF and (d) PCE.

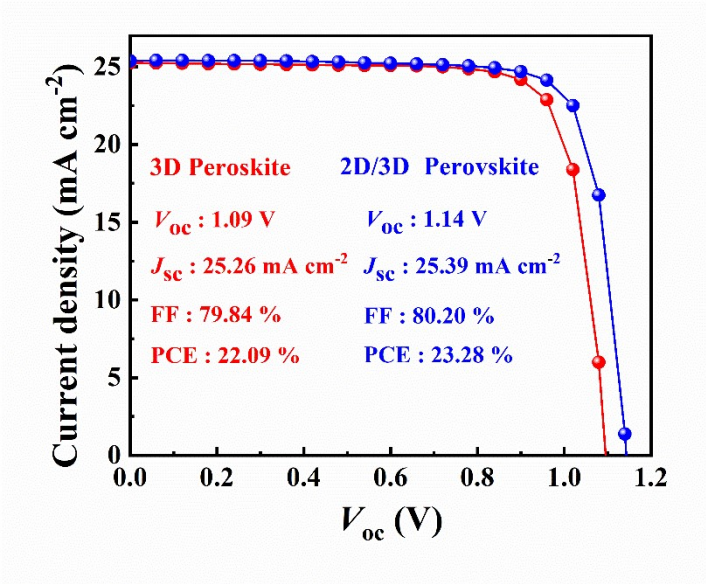

Fig. S7 *J-V* curves of 3D and 2D/3D PSCs based on 3D perovskite with a bandgap of 1.56 eV.

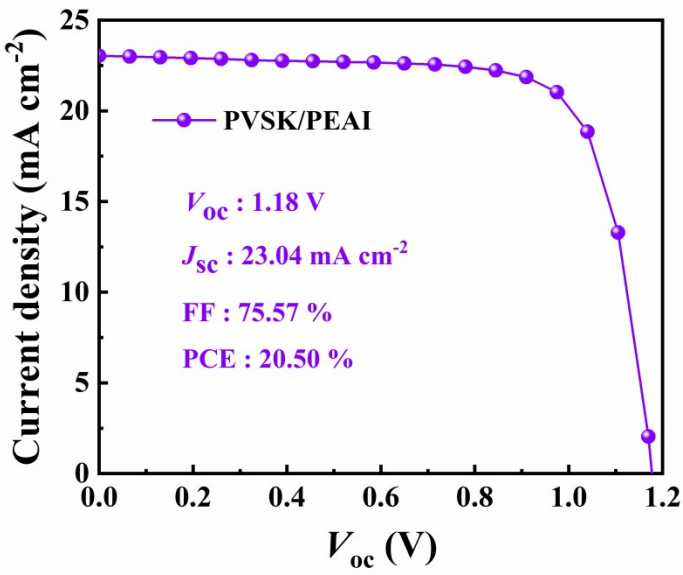

Fig. S8 *J-V* curve of PSCs with PEAI post-treatment.

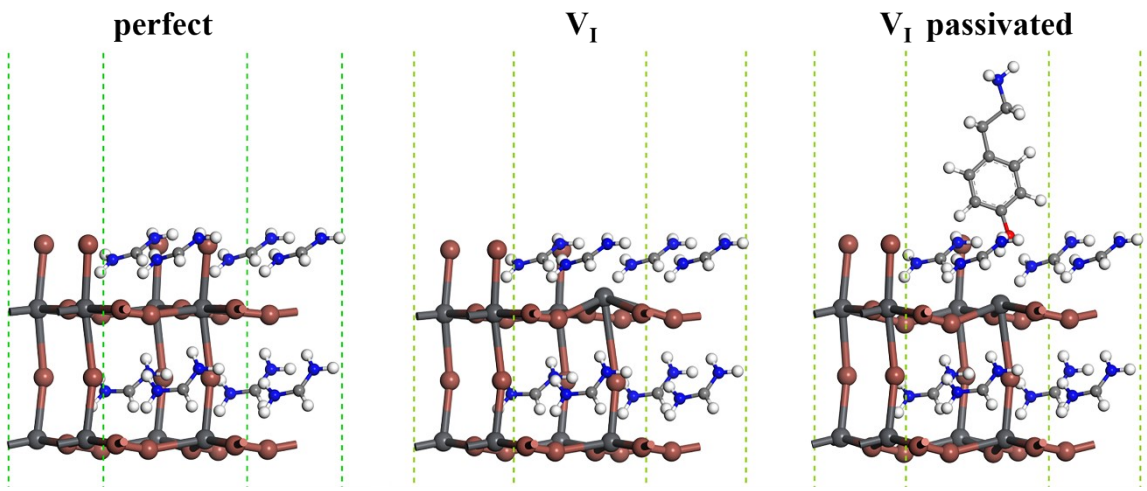

Fig. S9 Structural models of V_I for DFT calculation.

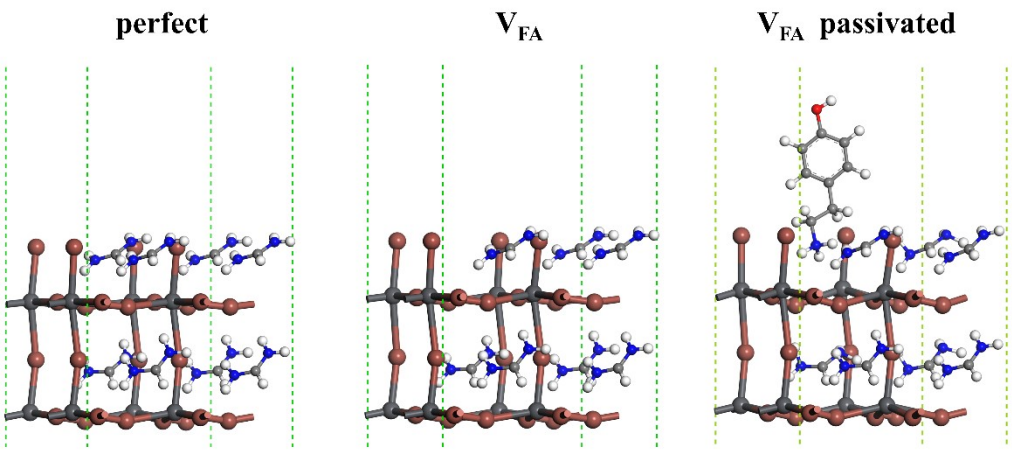

Fig. S10 Structural models of V_{FA} for DFT calculation.

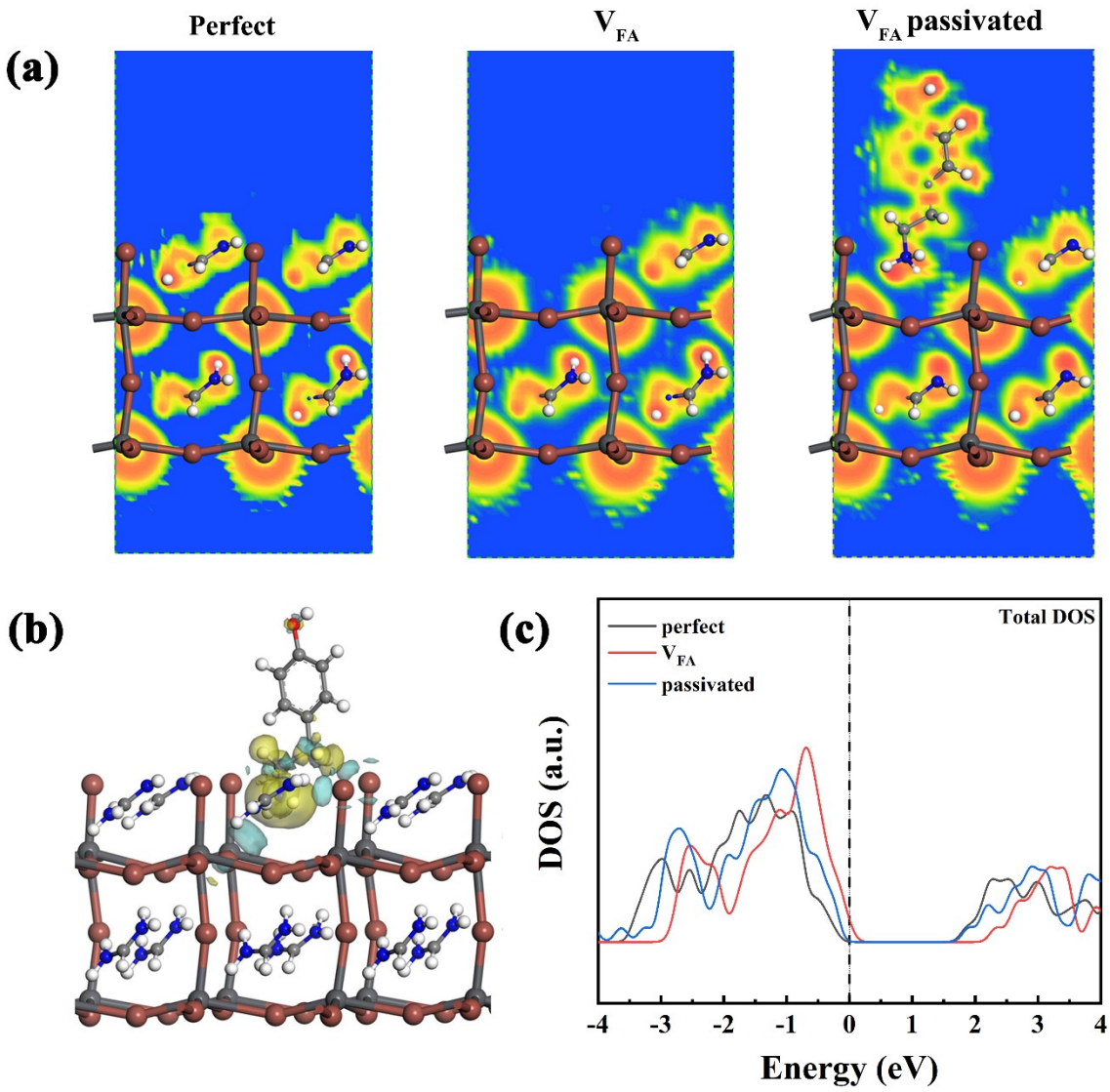

Fig. S11 DFT calculation for defect passivation on perovskite surface with OH-PEAI. (a) Electron localization function for perfect surface, with V_{FA}, and passivated defect. (b) Differential charge density when OH-PEAI fills into V_{FA}. The green and yellow isosurfaces represent the accumulation and loss of electron density, respectively. (c) The total DOS in each case.

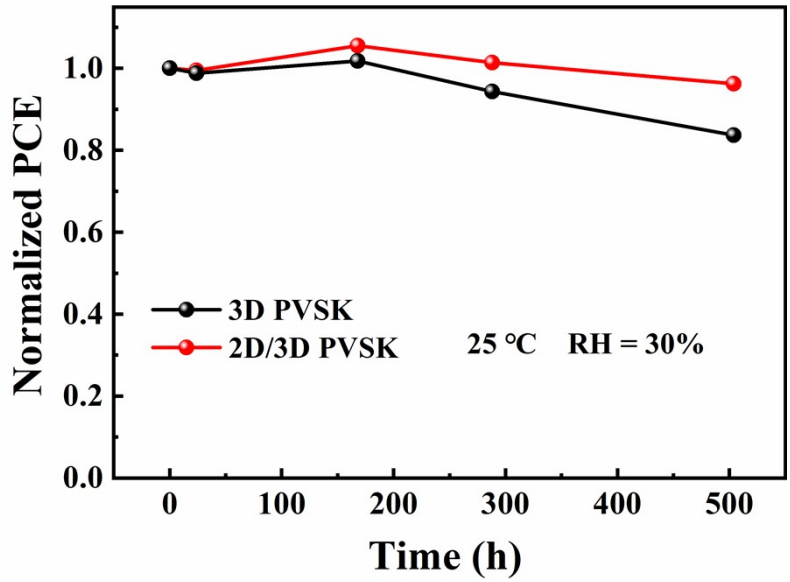

Fig. S12 The long-term stability of 3D and 2D/3D PSCs with the lower bandgap perovskite (1.56 eV, unencapsulated) at 30 % RH under dark conditions.

Table S1. Photovoltaic performance metrics of state-of-the-art 2D/3D PSCs with V_{oc} for bandgaps ranging from 1.58 ~1.63 eV

Perovskite	Architecture	E_g (eV)	V_{oc} (V)	PCE (%)	Ref.
$MAPbI_3$	p-i-n	1.58	1.20	20.14	S1
$(FAPbI_3)_{0.88}(CsPbBr_3)_{0.12}$	n-i-p	1.58	1.07	16.75	S2
$Cs_{0.05}(FA_{0.83}MA_{0.17})_{0.95}Pb(I_{0.83}Br_{0.17})_3$	n-i-p	1.60	1.11	18.51	S3
$MAPbI_3$	n-i-p	1.60	1.08	19.10	S4
$MAPbI_3$	n-i-p	1.60	1.06	18.0	S5
$Cs_{0.05}FA_{0.83}MA_{0.12}PbI_{2.62}Br_{0.38}$	p-i-n	1.60	1.18	21.31	S6
$Cs_{0.05}(FA_{0.83}MA_{0.17})_{0.95}Pb(I_{0.83}Br_{0.17})_3$	n-i-p	1.61	1.09	20.16	S7
$Cs_{0.05}(MA_{0.17}FA_{0.83})_{0.95}Pb(I_{0.83}Br_{0.17})_3$	n-i-p	1.61	1.187	21.80	S8
$(FAPbI_3)_{0.87}(MAPbBr_3)_{0.92}(CsPbI_3)_{0.08}$	n-i-p	1.61	1.19	20.82	S9
RbCsMAFA (I:Br = 0.83:0.17)	n-i-p	1.63	1.24	21.54	S10
$Rb_{0.05}Cs_{0.05}[(FA_{0.83}MA_{0.17})]_{0.9}Pb(I_{0.83}Br_{0.17})_3$	n-i-p	1.61	1.234	21.38	This work

Table S2. Fitting parameters for the transient photovoltage decay and time-resolved PL decay from 3D and 3D/2D perovskite films with different concentration of OH-PEAI.

Sample	A_1 (%)	τ_1 (ns)	A_2 (%)	τ_2 (ns)	τ_{ave} (ns)
pristine	6.31	4.55	93.69	59.26	58.39
2 mg/mL	32.83	58.09	67.17	200.13	153.50
4 mg/mL	23.01	60.73	76.99	232.27	185.90
6 mg/mL	27.76	49.26	72.24	185.20	147.46

Table S3. Photovoltaic parameters of the devices under difference scan directions (Reverse (1.3 V → 0 V) and Forward (0 V → 1.3 V)).

Devices	Scan Direction	V_{oc} (V)	J_{sc} (mA cm^{-2})	FF (%)	PCE (%)	H-index
3D PVSK	Reverse	1.16	22.68	73.24	19.26	12.46%
	Forward	1.13	23.23	64.16	16.86	
2D/3D PVSK	Reverse	1.23	22.80	75.83	21.18	0.09%
	Forward	1.22	23.00	75.44	21.16	

Note: H-index = ($PCE_{reverse}$ - $PCE_{forward}$)/$PCE_{reverse}$

Table S4. The calculated parameters of 2D/3D and 3D devices from EIS.

Devices	R_s **(Ω)**	R_{ct} **(Ω)**	R_{rec} **(Ω)**
3D PVSK	12.4	152	967
2D/3D PVSK	12.7	150	2420

Reference:

S1 J. Hu, C. Wang, S. Qiu, Y. Zhao, E. Gu, L. Zeng, Y. Yang, C. Li, X. Liu, K. Forberich, C. J. Brabec, M. K. Nazeeruddin, Y. Mai, F. Guo, *Adv. Energy Mater.*, 2020, **10**. 2000173

S2 J. Chen, J.-Y. Seo, N.-G. Park, *Adv. Energy Mater.*, 2018, **8**. 1702714

S3 P. Chen, Y. Bai, S. Wang, M. Lyu, J. H. Yun, L. Wang, *Adv. Funct. Mater.*, 2018, **28**, 1706923.

S4 M. H. Li, H. H. Yeh, Y. H. Chiang, U. S. Jeng, C. J. Su, H. W. Shiu, Y. J. Hsu, N. Kosugi, T. Ohigashi, Y. A. Chen, P. S. Shen, P. Chen, T. F. Guo, *Adv. Mater.*, 2018, **30**, 1801401.

S5 T. Ye, A. Bruno, G. Han, T. M. Koh, J. Li, N. F. Jamaludin, C. Soci, S. G. Mhaisalkar, W. L. Leong, *Adv. Funct. Mater.*, 2018, **28**. 1801654.

S6 C. Zhang, S. Wu, L. Tao, G. M. Arumugam, C. Liu, Z. Wang, S. Zhu, Y. Yang, J. Lin, X. Liu, R. E. I. Schropp, Y. Mai, *Adv. Energy Mater.*, 2020, **10**. 2002004.

S7 P. Li, Y. Zhang, C. Liang, G. Xing, X. Liu, F. Li, X. Liu, X. Hu, G. Shao, Y. Song, *Adv. Mater.*, 2018, **30**, 1805323.

S8 S. Wang, F. Cao, Y. Wu, X. Zhang, J. Zou, Z. Lan, W. Sun, J. Wu, P. Gao, *Mater. Today Phys.*, 2021, **21**. 100543.

S9 A. A. Sutanto, P. Caprioglio, N. Drigo, Y. J. Hofstetter, I. Garcia-Benito, V. I. E. Queloz, D. Neher, M. K. Nazeeruddin, M. Stolterfoht, Y. Vaynzof, G. Grancini, *Chem*, 2021, **7**, 1903.

S10 G. Yang, Z. Ren, K. Liu, M. Qin, W. Deng, H. Zhang, H. Wang, J. Liang, F. Ye, Q. Liang, H. Yin, Y. Chen, Y. Zhuang, S. Li, B. Gao, J. Wang, T. Shi, X. Wang, X. Lu, H. Wu, J. Hou, D. Lei, S. K. So, Y. Yang, G. Fang, G. Li, *Nat. Photonics*, 2021, **15**, 681–689.